Supporting Information

Ultrahigh water permeation with high multivalent metal ions rejection through graphene oxide membranes

Fangfang Dai,‡[a] Feng Zhou,‡[b] Junlang Chen,[a] Shanshan Liang,*[c] Liang Chen,*[a] and Haiping Fang[c]

[a] *Department of Optical Engineering, Zhejiang Prov Key Lab Carbon Cycling Forest Ecosy, College of Environmental and Resource Sciences, Zhejiang A&F University, Hangzhou 311300, China.*

[b] *Radiation Monitoring Technical Center of Ministry of Environmental Protection, State Environmental Protection Key Laboratory of Radiation monitoring, Key Laboratory of Radiation Monitoring of Zhejiang Province, Hangzhou 310012, China.*

[c] *Department of Physics, East China University of Science and Technology, Shanghai 200237, China.*

Contents

PS1: Materials and methods

Fabrication of GO suspension

Graphene oxide (GO) were prepared from natural graphite powder via a modified Hummers method[S1-S3]. Graphite powders were put into concentrated H_2SO_4, $K_2S_2O_8$, and P_2O_5 solution with continuous stirring for several hours. Then the mixture was diluted with deionized water (DI), centrifuged, and washed with DI water. After dry, the preoxidized graphite was obtained. Then, they were further oxidized in concentrated H_2SO_4 and $KMnO_4$, diluted with DI water, followed by the addition of 30% H_2O_2. The product was centrifuged and washed with 1:10 HCl aqueous solution and DI water sequentially to remove ion species. At last, the concentration of the as-prepared GO suspension (4 mg/mL) was diluted to about 7.5 mg/L with DI water.

GO Membrane Preparation

GO membranes were prepared from the 7.5 mg/L GO suspensions on the mixed cellulose ester (MCE) substrates under the applied pressure of 1 bar using vacuum filtration. Then the GO membranes without drying treatment were prepared to conduct the multivalent metal ions rejection experiments. The GO membranes with four thickness of about 100 nm, 200 nm, 400 nm and 800 nm were prepared by using 20 mL, 40 mL, 80 mL and 160 mL of 7.5 mg/L GO suspensions, which were denoted as GO-20, GO-40, GO-80 and GO-160 membranes, respectively.

GO membranes fabricated by conventional drop-casting method were prepared by drop-casting the GO suspension (4 mg/mL, 1 mL) droplets onto a smooth paper substrate. The GO membranes fabricated by conventional drop-casting method were drying thoroughly at 60 ºC for 12 hours. After that, they were peeled off, rinsed and soaked with DI water for more than half an hour to remove the absorbed metal ions

(especially the Mn^{2+}, see Fig. S1), then dried in a dry dish at room temperature for three days. These drop-casting GO membranes were used for ion controlling experiments.

Filtration experiment

5~500 mg/L different multivalent metal cations ($FeCl_3$, $CuSO_4$, $Pb(NO_3)_2$ or $ZnSO_4$) solutions were added into the feed side after the GO membrane were prepared using vacuum filtration, respectively. Under the applied pressure of 1 bar, the salt solutions were filtered through GO membranes. Filtrates were collected when the filtration process became steady. The water permeance (J_w) was measured by using the following equation (1):

$$J_w = \frac{V}{\Delta t \times A \times P} \quad (1)$$

where J_W is the water permeance (L m^{-2} h^{-1} bar^{-1}), V is the volume of the filtrate (L), A is the effective membrane area (m^2), Δt is the permeation time (h) and the P is the applied pressure (bar).

The feed volume is 100 mL, applied pressure is 1 bar, and effective filtration area is 11.74 cm^2.

The rejection rate (R) for the multivalent ions were calculated from the concentration of the feed and permeate solutions. The rejection rate was measured by using the following equation (2):

$$R = (1 - \frac{C_P}{C_f}) \times 100\% \quad (2)$$

where C_p and C_f are the concentration of permeation and feed ions solution which were measured by inductive coupled plasma-optical emission spectrometry (ICP-OES), respectively.

Three parallel permeation tests were performed to obtain the average values of water permeance and rejection rate.

Adsorption experiment

GO membranes were prepared from 40 mL, 7.5 mg/L GO suspensions on substrates using vacuum filtration. Then, 100 mL, 5 mg/L $FeCl_3$, $Pb(NO_3)_2$, $ZnSO_4$, and $CuSO_4$ solutions were added to the feed side, respectively. These salt solutions under ambient conditions (without vacuum filtration) were stirred with a blender at ~180 RPM. Next, samples were collected at different pre-determined time intervals in 120 min to evaluate the residual salt concentrations of the solutions. We noted that the salt solutions in the feed side permeated very slowly though the GO membranes due to their own gravity, the filtrates were only ~ 5 mL within 120 min. Therefore, the effect of the small volume of filtrates on the salt concentration during the adsorption experiments could be negligible.

The adsorption efficiency (AE) was defined by using the following equation (3):

$$AE = \left(1 - \frac{C_a}{C_0}\right) * 100\% \quad (3)$$

where, Co and Ca is the initial feed concentration and the concentration of salts after adsorption equilibrium, respectively.

Characterizations

As-prepared GO membranes were characterized by scanning electron microscope (SEM, Hitachi, S-4800) and X-ray diffraction (XRD, Siemens, 08DISCOVER, λ=0.15418 nm). The concentrations of ions solutions were determined using PS7800 inductive coupled plasma optical emission spectrometer (ICP-OES).

Calculation Methods

The B3LYP [S4,S5] method is used to study the intermolecular interactions. For geometry optimizations, the double-ζ basis was employed, and a d-polarization function was added (marked with 6-31 G(d)). The pseudopotential function with Lanl2dz is introduced into the basis set for Fe^{3+} ion. Two graphene surfaces of 15.69 × 12.26 $Å^2$ were used for the DFT study, which were large enough to obtain results with a tolerable error. All calculations were carried out using the Gaussian-09 program[S6].

PS2: XPS spectra for the GO membrane

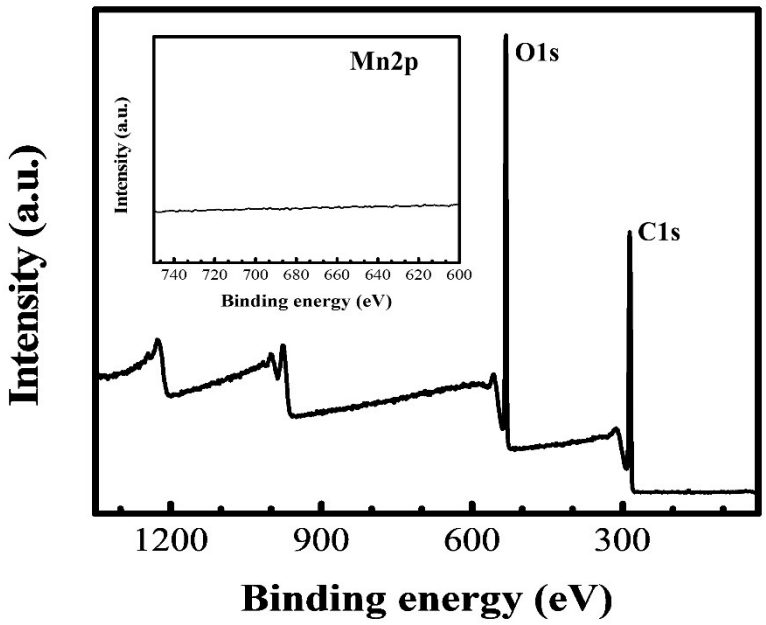

Supplementary Fig. S1. X-ray photo electron spectrometer (XPS) spectra of the GO membrane.

Elements in the GO membrane was characterized using X-ray photoelectron spectrometer spectra (XPS). As shown in Fig. S1, for the pristine GO membrane, Mn^{2+} in the membrane were undetected (see insert of Fig. S1), indicating there is almost no residual Mn^{2+} ions.

PS3: Filtration performance of the nanofiltration membranes reported in literature in terms of water permeances and rejection rates for multivalent ions

Supplementary Table S1 Comparisons of different nanofiltration membranes in water permeances and rejection rates for multivalent metal ions in literature.

Material	Solution	Water permeance (L m^{-2} h^{-1} bar^{-1})	Rejection rate	Membrane Type
Noria–PEI IP[f1]	$MgSO_4$	27.6	97.7%	TFC/TFN
TMC/CNC-PES [f2]	$MgSO_4$	34.1	82%	TFC/TFN
TMC/SWCNTS-PES [f3]	$MgCl_2$	38.0	92.5%	TFC/TFN
TMC/ PVC UF [f4]	$MgCl_2$	15.2	98.6%	TFC/TFN
TMC/MWCNTS-PES [f5]	$MgCl_2$	17.6	78%	TFC/TFN
PIP-TMC/TA-DETA/ PSF [f6]	$MgCl_2$	10.5	70.0%	TFC/TFN
TMC/UCN [f7]	$MgSO_4$	17.6	79.8%	TFC/TFN
TMC/PDA/PES [f8]	$MgCl_2$	11.4	12.3%	TFC/TFN
PDA-MWCNTS +TMC/PSF [f9]	$MgCl_2$	15.3	91.4%	TFC/TFN
PVA-TMC/PSF [f10]	$MgCl_2$	13.4	6.5%	TFC/TFN
DCPO-IPDC /BTEC/PSF [f11]	$MgCl_2$	17.9	92.1%	TFC/TFN
BPF/PIP-TMC/PES [f12]	$MgCl_2$	11.9	49.4%	TFC/TFN

PVA-TMC/PSF [f13]	$MgCl_2$	24.9	91.2%	TFC/TFN
Dow-Filmtec NF 270 [f14]	$MgCl_2$	13.2	60.0%	TFC/TFN
Dow-Filmtec NF 90 [f15]	$MgCl_2$	6.7	96.0%	TFC/TFN
PSE-GO-DMF [f16]	Cr^{3+}	13.5	91.2%	TFC/TFN
HPEI-GO 10 [f17]	Ni^{2+}	4.2	94.6%	TFC/TFN
Chitosan PES composite membrane [f18]	$Pb(NO_3)_2$	3.5	93.1%	TFC/TFN
PDA/TFC composite membrane [f19]	$Pb(NO_3)_2$	3.5	91.1%	TFC/TFN
PDA/PEI membranes [f20]	$Pb(NO_3)_2$	50	79.0%	TFC/TFN
TFC /PES support [f21]	$NiCl_2$	2.5	66.0%	TFC/TFN
GO/TiO2-PDDA [f22]	$MgCl_2$	51.2	93.2%	2D materials
TMV [f23]	$MgSO_4$	62.0	98.0%	2D materials
GO/QDs [f24]	$CdCl_2$	17.36	29.4%	2D materials
GO/PAN [f25]	$MgCl_2$	17.0	37.0%	2D materials
MWNT-rGO/PVDF [f26]	$MgCl_2$	11.3	9.6%	2D materials
CNT-PA [f27]	$MgSO_4$	12.0	98.3%	2D materials
UiO-66 [f28]	$MgCl_2$	0.14	98.0%	2D

				materials
rGO/PVDF [f29]	$MgCl_2$	3.26	20%	2D materials
Mxene [f30]	$MgCl_2$	9	82%	2D materials
ZIF-PA [f31]	$MgSO_4$	45.5	40%	2D materials
UV-GO [f32]	$MgCl_2$	2.8	78.4	2D materials
MoS2 [f33]	$Cu(NO_3)_2$	2.5	90.0	2D materials
MOF/Chitosan [f34]	$MgCl_2$	3.2	93.0%	2D materials
COF [f35]	$MgCl_2$	41.5	90.2%	2D materials
GO	$FeCl_3$ $CuSO_4$ $Pb(NO_3)_2$ $ZnSO_4$	75.2 56.6 46.6 48.7	99.9% 97.8% 86.9% 83.0%	This work

f1. Zhai, Z., et al., Fabrication of advanced nanofiltration membranes with nanostrand hybrid morphology mediated by ultrafast Noria–polyethyleneimine codeposition. *J. Mater. Chem. A*, **2018**, *6*(42), 21207-21215.

f2. Wang, J.-J., et al., Nanofiltration membranes with cellulose nanocrystals as an interlayer for unprecedented performance. *J. Mater. Chem. A*, **2017**, *5*(31), 16289-16295.

f3. Zhu, Y., et al., Single-Walled Carbon Nanotube Film Supported Nanofiltration Membrane with a Nearly 10 nm Thick Polyamide Selective Layer for High-Flux and High-Rejection Desalination. *Small*, **2016**, *12*(36), 5034-5041.

f4. Liu, S., et al., One-step constructed ultrathin Janus polyamide nanofilms with opposite charges for highly efficient nanofiltration. *J. Mater. Chem. A,* **2017**, *5*(44), 22988-22996.

f5. Wu, M.-B., et al., Thin film composite membranes combining carbon nanotube intermediate layer and microfiltration support for high nanofiltration performances. *J. Membr. Sci.*, **2016**, *515*, 238-244.

f6. Zhang, X., et al., Polyphenol Coating as an Interlayer for Thin-Film Composite Membranes with Enhanced Nanofiltration Performance. *ACS Appl. Mater. Inter.*, **2016**, *8*(47), 32512-32519.

f7. Soyekwo, F., et al., Cellulose nanofiber intermediary to fabricate highly-permeable ultrathin nanofiltration membranes for fast water purification. *J. Membr. Sci.*, **2017**, *524*, 174-185.

f9. Li, Y., et al., Preparation of thin film composite nanofiltration membrane with improved structural stability through the mediation of polydopamine. *J. Membr. Sci*, **2015**, *476*, 10-19.8

f9. Zhao, F.-Y., et al., High-Flux Positively Charged Nanocomposite Nanofiltration Membranes Filled with Poly(dopamine) Modified Multiwall Carbon Nanotubes. *ACS Appl. Mater. Inter.*, **2016**, *8*(10), 6693-6700.

f10. Wang, T., et al., Fabrication of high flux nanofiltration membrane via hydrogen bonding based co-deposition of polydopamine with poly(vinyl alcohol). *J. Membr. Sci.*, **2018**. *552*, 222-233.

f11. Zhao, Y., et al., Preparation of a highly permeable nanofiltration membrane using a novel acyl chloride monomer with -$PO(Cl)_2$ group. *Desalination*, **2018**, *431*, 56-65.

f12.Tang, Y.-J., et al., Tailoring the polyester/polyamide backbone stiffness for the fabrication of high performance nanofiltration membrane. *J. Membr. Sci.*, **2017**, *541*, 483-491.

f13.Tan, Z., et al., Polyamide membranes with nanoscale Turing structures for water purification. *Science*, **2018**, *360* (6388), 518-521.

f14. Fang, W., L. Shi, and R. Wang, Mixed polyamide-based composite nanofiltration hollow fiber membranes with improved low-pressure water softening capability. *J. Membr. Sci.*, **2014**, *468*, 52-61.

f15. Liu, C., L. Shi, and R. Wang, Crosslinked layer-by-layer polyelectrolyte nanofiltration hollow fiber membrane for low-pressure water softening with the presence of SO_4^{2-} in feed water. *J. Membr. Sci.*, **2015**, *486*, 169-176.

f16. Mukherjee, R., P. Bhunia, and S. De, Impact of graphene oxide on removal of heavy metals using mixed matrix membrane. *Chem. Eng. J.*, **2016**, *292*, 284-297.

f17.Z hang, Y., et al., Layer-by-layer construction of graphene oxide (GO) framework composite membranes for highly efficient heavy metal removal. *J. Membrane Sci.*, **2016**, *515*, 230-237.

f18.Zhang, S., et al., Thin Film Interfacial Cross-Linking Approach To Fabricate a Chitosan Rejecting Layer over Poly(ether sulfone) Support for Heavy Metal Removal. *Ind. Eng. Chem. Res.*, **2015**, *54*(1), 472-479.

f19.Wang, T., et al., Large-eddy simulations of the multi-mode Richtmyer–Meshkov instability and turbulent mixing under reshock. *High Energ. Dens. Phys.*, **2016**, *19*, 65-75.

f20. Hebbar, R.S., et al., Fabrication of polydopamine functionalized halloysite nanotube/polyetherimide membranes for heavy metal removal. *J. Mater. Chem. A*, **2016**, *4*(3), 764-774.

f21. Mahdavi, H., F. Razmi, and T. Shahalizade, Polyurethane TFC nanofiltration membranes based on interfacial polymerization of poly(bis-MPA) and MDI on the polyethersulfone support. *Sep. Purif. Technol.*, **2016**, *162*, 37-44.

f22. Zhang, M., et al. Controllable ion transport by surface-charged graphene oxide membrane. *Nat. Commun.*, **2019**, *10*, 1253.

f23. Gui, L., et al. Ultrafast Ion Sieving from Honeycomb-like Polyamide Membranes Formed Using Porous Protein Assemblies. *Nano Lett.*, **2020***, 20* (8)*,* 5821-5829.

f24. Zhao, G., et al. High flux nanofiltration membranes prepared with a graphene oxide homo-structure. *J. Membr. Sci.*, **2019**, *585*, 29-37.

f25. Zhang, M., et al. Effect of substrate on formation and nanofiltration performance of graphene oxide membranes. *J. Membr. Sci.*, **2019**, *574*, 196-204.

f26. Han, Y., Y. Jiang, and C. Gao, High-Flux Graphene Oxide Nanofiltration Membrane Intercalated by Carbon Nanotubes. *ACS Appl. Mater. Inter.*, **2015**, *7*(15), 8147-8155.

f27. Gong, G., et al., New Insights into the Role of an Interlayer for the Fabrication of Highly Selective and Permeable Thin-Film Composite Nanofiltration Membrane. *ACS Appl. Mater. Inter.*, **2019**, *11*(7), 7349-7356.

f28. Liu, X., et al. Highly water-stable zirconium metal-organic framework UiO-66 membranes supported on alumina hollow fibers for desalination *J. Am. Chem. Soc.*,137(2015), 6999-7002.

f29. Han, Y. et al. Ultrathin graphene nanofiltration membrane for water purification. *Adv. Funct. Mater.* **2013**, *23*, 3693-3700.

f30. Meng B. et al. Fabication of surface-charged MXene membrane and its application for desalination. *J. Membr. Sci.*, **2021**, *623*, 119076.

f31. Wang, Z., et al. Nanoparticle-templated nanofiltration membranes for ultrahigh performance desalination. *Nat. Commun.*, **2018**, *9* (1), 2004.

f32. Chong, J.Y., et al. UV-enhanced sacrificial layer stabilised graphene oxide hollow fiber membranes for nanofiltration. *Sci. Rep*. **2015**, *5*, 15799.

f33. Zhang, H., et al. Construction of MoS_2 composite membranes on ceramic hollow fibers for efficient water desalination. *J. Membr. Sci.*, **2019**, *592*, 117369.

f34. Ma, X.-H., et al. A facile preparation of novel positively charged MOF/chitosan nanofiltration membranes. *J. Membr. Sci.*, **2017**, *525*, 269-276.

f35. Yangk, H., et al. Covalent organic framework membranes through a mixed0dimensional assembly for molecular separation. *Nat. Commun.* **2019**, *10*, 2101.

PS4: Effect of concentration of $FeCl_3$ solution on filtration performances

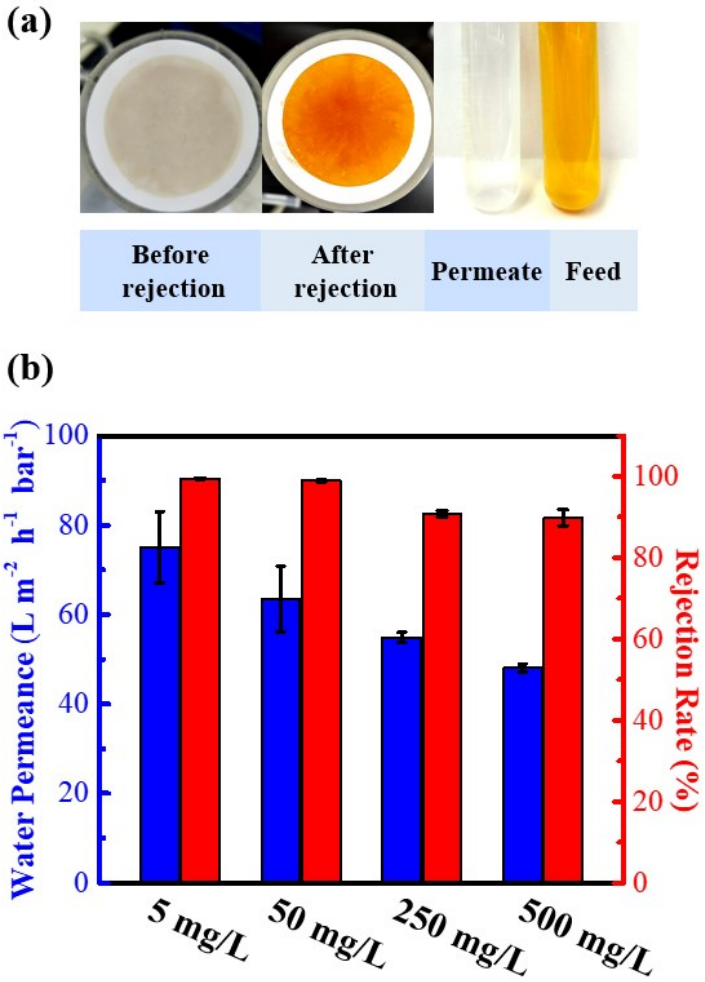

Supplementary Fig. S2. (a) Digital images of the GO membranes before and after rejection for 250 mg/L $FeCl_3$ solution; and $FeCl_3$ solution added in the feed side and the permeate though the GO membranes. **(b)** Water permeances and rejection rates of the GO membranes as a function of concentration of $FeCl_3$ solutions.

PS5: Adsorption experiment for the GO membrane in high concentration solution

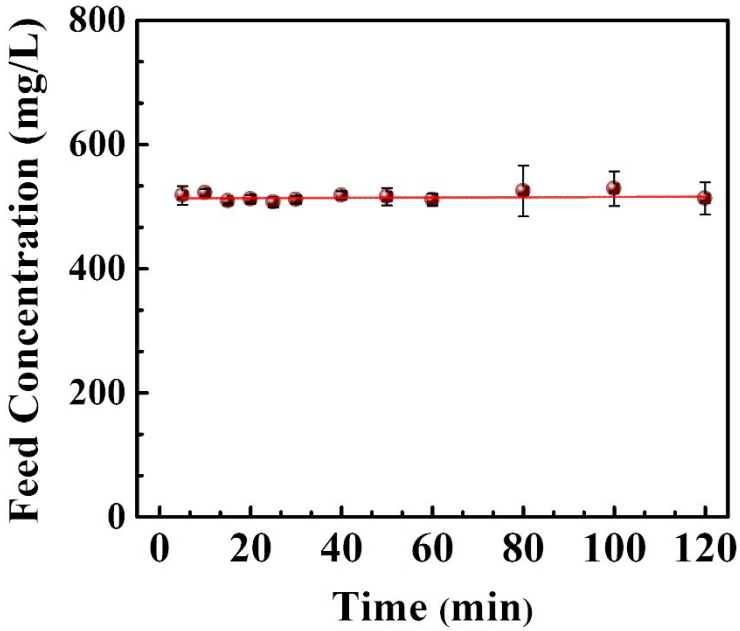

Supplementary Fig. S3. Concentration variations of 500 mg/L $FeCl_3$ solution adsorbed by the GO membranes as a function of adsorption time.

PS6: Experimental setup for the mass balance experiment

The mass balance experiment for 500 mg/L $FeCl_3$ solution rejection has been investigated to justify the mass balance of feed and permeate during the rejection experiments. As shown in Fig. S4(a), during the filtration process, we recycled the filtrates into the feed side to test the change of salt concentration in the feed, which is referred to the method reported previously [S7].

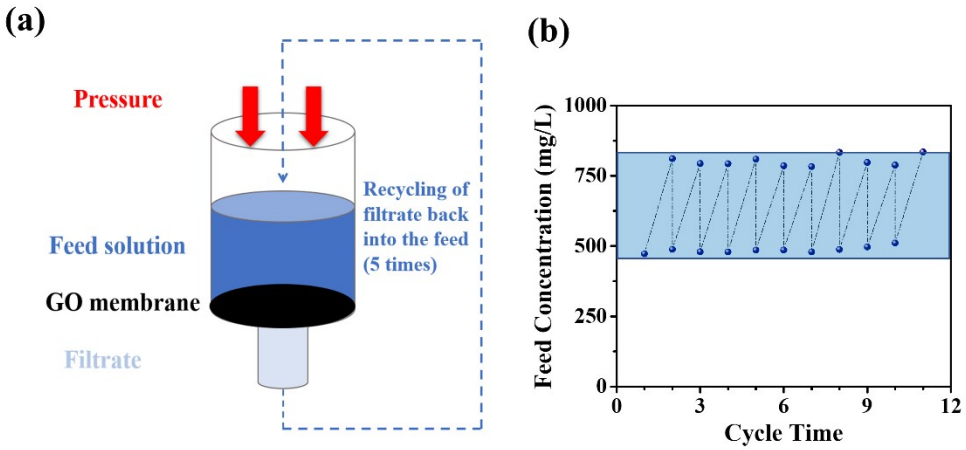

Supplementary Fig. S4. (a) Schematic of operation process for semi-continuous mass balance experiment and **(b)** Variations of feed concentration with cycle numbers. Feed volume is 200 mL, operation pressure is 1 bar, and effective filtration area is 11.74 cm^2.

In details, 200 mL $FeCl_3$ solution was added to the feed side, then the salt solution was filtered through the GO membranes under a pressure of 1 bar. When the filtrate was collected to approximately 80 mL solution, the filtrate was recycled into the feed side. The feed concentrations of the $FeCl_3$ solution before and after recycling filtrate were measured, respectively. As shown in Fig. S4(b), the periodic variation of salt concentration in the feed was about 500~800 mg/L. In one cycle, the salt concentrations in feed side significantly increased from ~500 mg/L to ~800 mg/L, indicating an effective rejection rather than adsorption by our membranes. Moreover, a stable rejection for the $FeCl_3$ solution was presented from the stable and periodic variations

of salt concentration, even though concentration polarization was enhanced due to the increase of salt concentrations in the feed side.

PS7: Stability experimental for the GO membrane

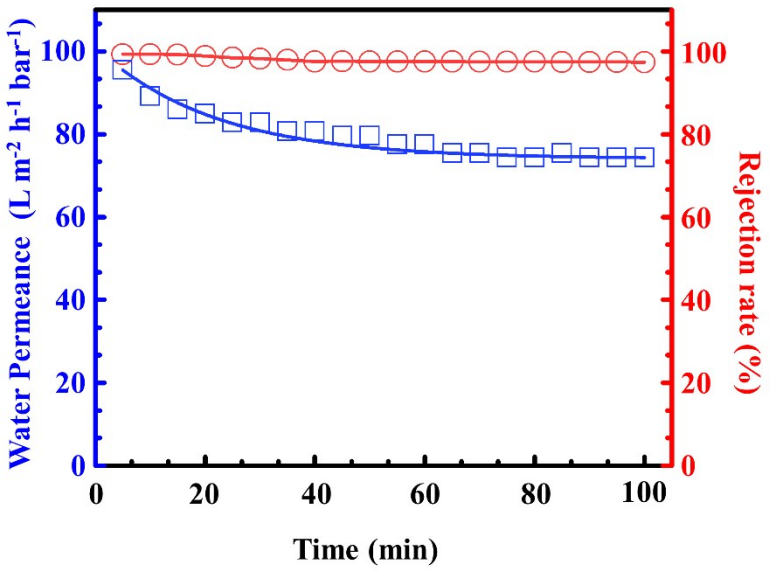

Supplementary Fig. S5. Variations of water permeance and rejection rate of 5 mg/L $FeCl_3$ solution through GO membranes as a function of filtration time. Blue and red lines correspond to water permeances and rejection rates, respectively.

PS8: Experimental setup for long-term experiment

100 mL, 500 mg/L $FeCl_3$ solution was added into the feed side, after the GO membrane were prepared using vacuum filtration. Under a pressure of 1 bar, the salt solutions were filtered through GO membranes. 30 mL filtrates were collected after 20 min when the filtration process became steady. Then, removed the residual salt solution, rinsed the GO membrane in the feed side for surface cleaning, and added another 30 mL DI water into the feed side, kept still before subsequent permeation of the DI water for filtration cleaning. Repeated the filtration process three times per day. The long-term test was conducted for 5 days, as shown in Fig. S6.

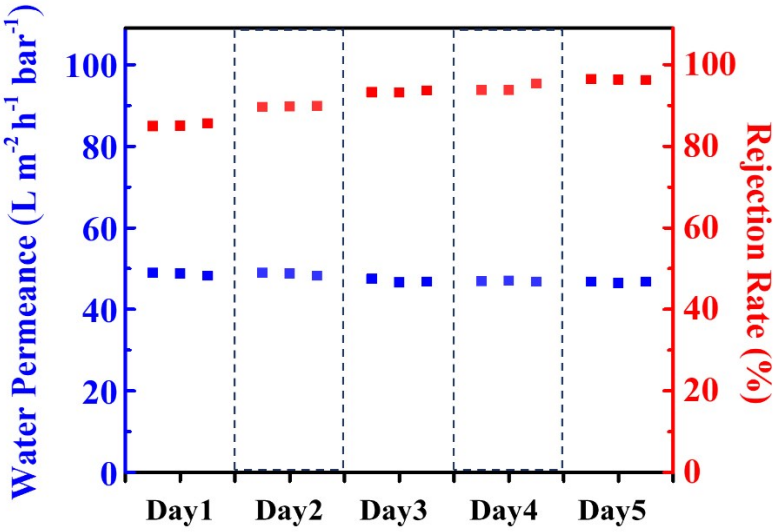

Supplementary Fig. S6. Long-term performance measurements of the GO membranes for 500 mg/L $FeCl_3$ solution for 5 days.

PS9: SEM images of GO membranes prepared by vacuum filtration with different vacuum loading

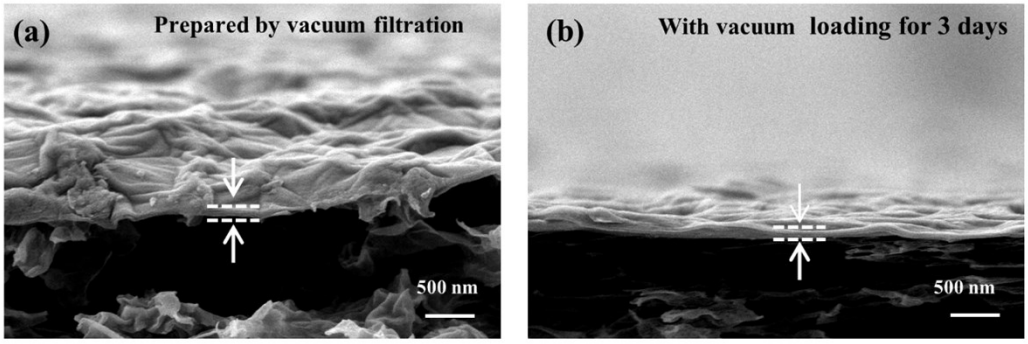

Supplementary Fig. S7. Cross-sectional SEM images of GO membranes. **(a)** Initial GO membrane prepared by vacuum filtration within 0.5 h. **(b)** GO membrane with vacuum loading for 3 days.

Fig. S7 shows that the cross-sectional SEM images of initial GO membrane prepared by vacuum filtration within 0.5 h, and the membrane with vacuum loading for 3 days. It can be found that the thickness of the GO membranes with long-term vacuum is smaller and the structure of the GO membranes is indeed more compacted than initial GO membrane prepared by vacuum filtration.

PS10: XRD of GO membranes prepared by vacuum filtration with different vacuum loading

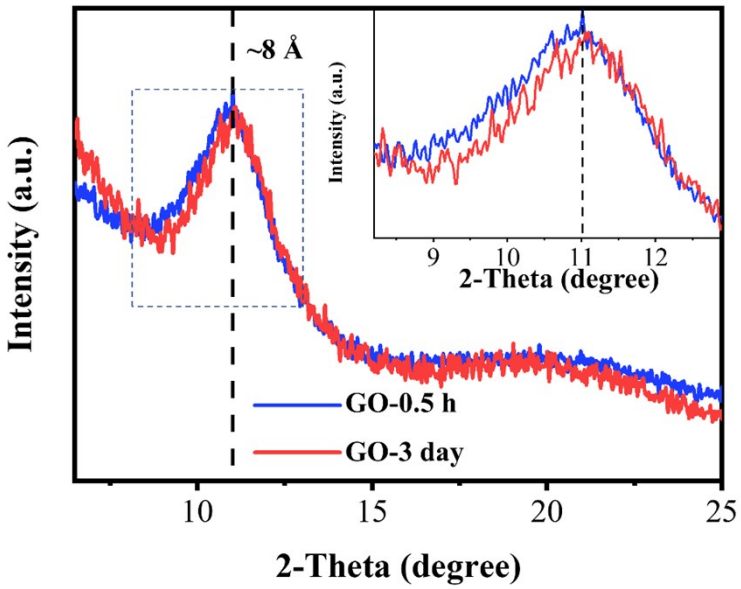

Supplementary Fig. S8. X-ray diffraction for dry GO membranes prepared by vacuum filtration within 0.5 h, and the membrane with vacuum loading for 3 days, respectively.

PS11: Experimental setup for high pressure experiment

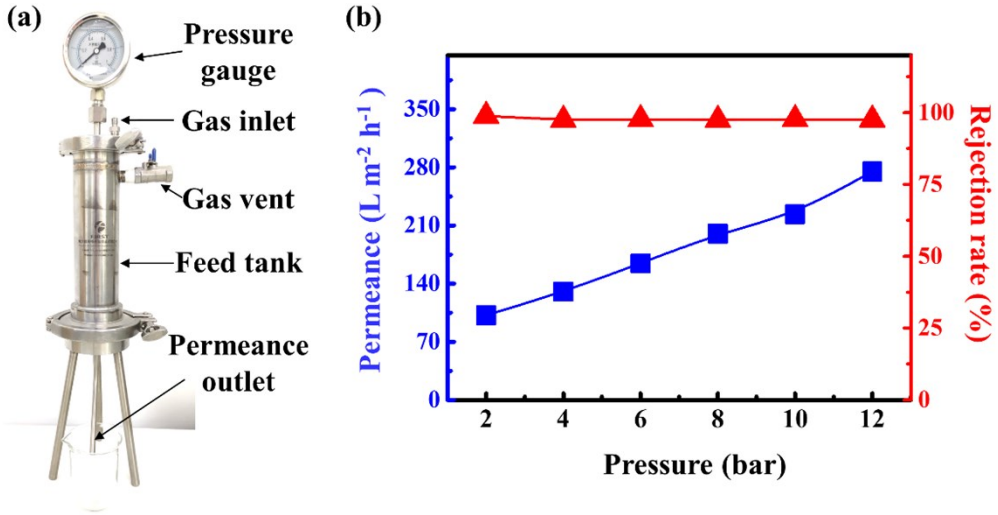

Supplementary Fig. S9. (a) Digital image of dead-end pressure filtration cell. **(b)** Filtration performance of the GO membranes for $FeCl_3$ solution with high pressure in the range of 2 to 12 bar.

PS12: SEM characterization for the GO membranes with different thickness

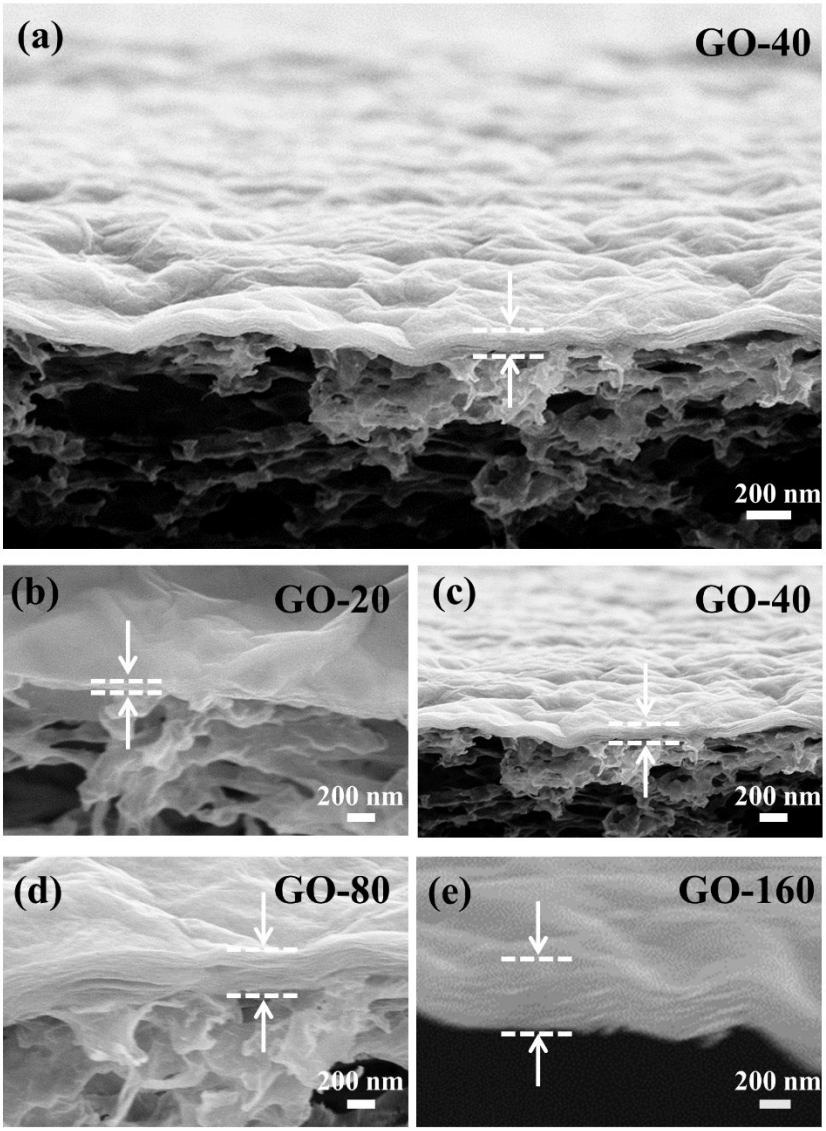

Supplementary Fig. S10 Cross-sectional SEM images of the GO membranes with different thicknesses. **(a)** and **(c)** Cross-sectional SEM images of the GO-40 membrane. **(b)**, **(d)**, and **(e)** Cross-sectional SEM images of the GO-20, GO-80, and GO-160 membranes, respectively.

PS13: Effect of membrane thickness on $FeCl_3$ permeation behavior

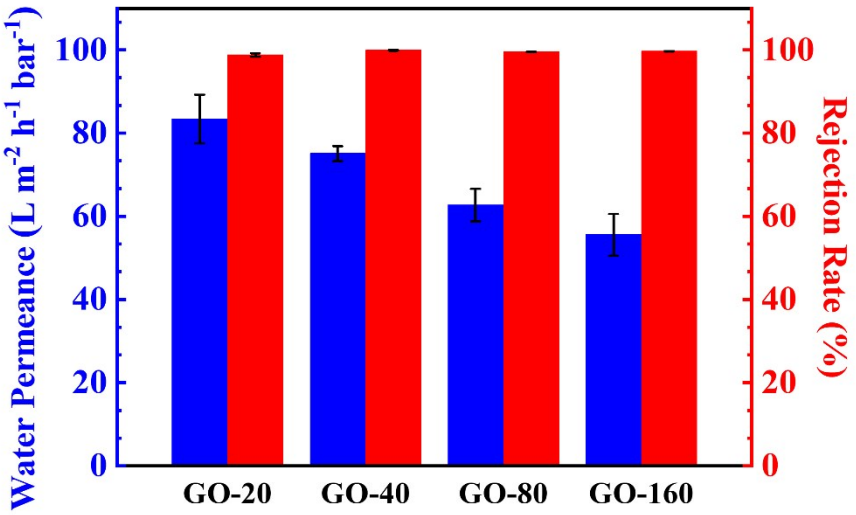

Supplementary Fig. S11. Water permeances and rejection rates of 5 mg/L $FeCl_3$ solutions through the GO membranes as a function of thickness.

PS14: Experimental setup for X-ray diffraction detection

The GO membranes (prepared by the vacuum method without drying treatment and conventional drop-casting method) were immersed in 5 mg/L different solutions ($FeCl_3$, $Pb(NO_3)_2$, $ZnSO_4$ and $CuSO_4$) at room temperature for half an hour, respectively. Then the wet membranes saturated with salt solution were removed and analysed by X-ray diffraction. The interlayer spacings of the GO membranes prepared by conventional drop-casting method in various solutions are shown in Fig. S12.

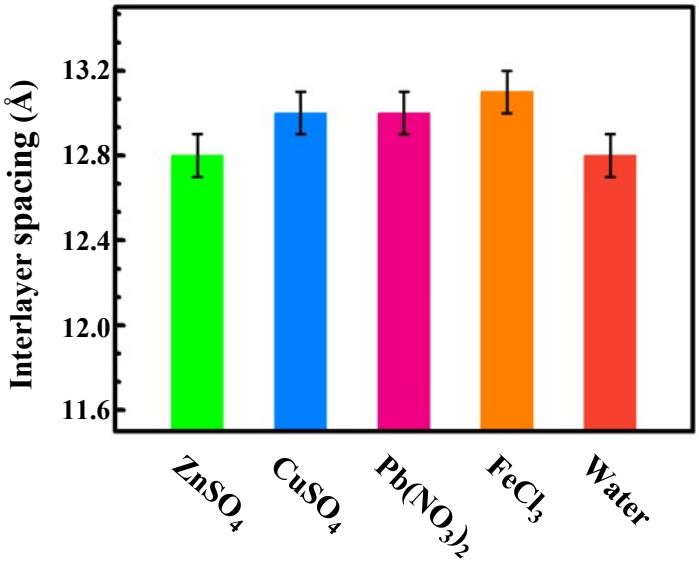

Supplementary Fig. S12. Interlayer spacings of the GO membranes fabricated by conventional drop-casting methods immersed in different multivalent ions solutions. Error bars indicate the standard deviation from three different samples.

We fabricated GO membranes by vacuum filtration, followed by drying at 60 ºC for 12 hours. These GO membranes were analysed by X-ray diffraction. As shown in Fig. S13, for the GO membranes prepared by vacuum filtration with drying treatment, the interlayer spacing were 8.0 Å and 13.0 Å for dry GO membrane and GO membrane immersed in pure water, consistent with the results of drop-casting method.

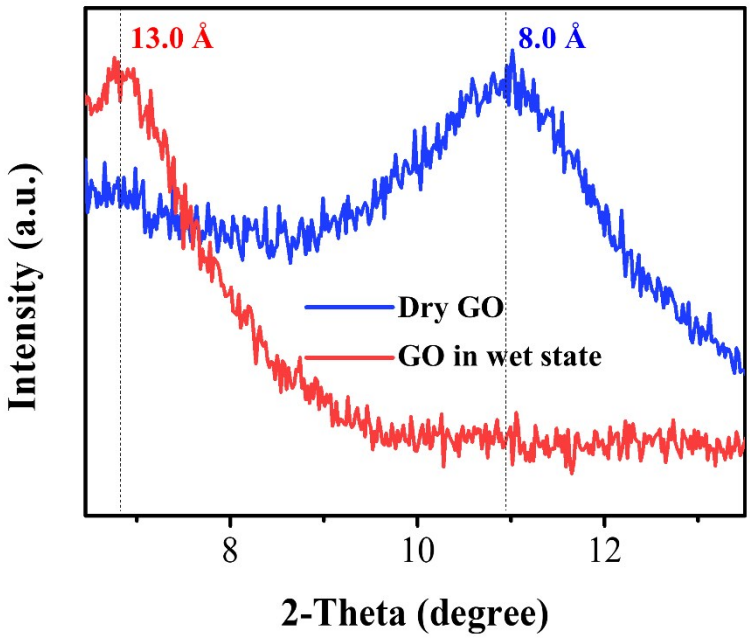

Supplementary Fig. S13. X-ray diffraction for GO membranes prepared by vacuum filtration with drying treatment. Blue and red lines correspond to XRD patterns of dry GO membranes, and GO membranes immersed in pure water (GO membranes in wet state), respectively.

For the $ZnSO_4$-controlled GO membranes or the $FeCl_3$-controlled GO membranes, the GO membranes were soaked in pure water for half an hour, and then immersed to $ZnSO_4$ or $FeCl_3$ solutions for half hour for pretreatment. The $ZnSO_4$-controlled GO membranes or the $FeCl_3$-controlled GO membranes were toke out and immersed to mixed salt solutions included 5 mg/L $ZnSO_4$ or $FeCl_3$ together with other 5 mg/L solutions ($Pb(NO_3)_2$, $CuSO_4$, $FeCl_3$ or $ZnSO_4$) for half hour. Finally, the membranes were removed from the mixed salt solutions and analysed by X-ray diffraction. The results are shown in the Fig 4 (b) and (d) for the interlayer spacings of the $ZnSO_4$-controlled GO membranes or the $FeCl_3$-controlled GO membranes, respectively, in the main text.

PS15: UV absorption spectral experiments

The UV absorption spectra of GO and GO in $FeCl_3$ solution are showed in Fig. S14. The UV spectrum of GO at ~ 230 nm, which is assigned to a conjugate double bond of the aromatic group that easily generated π-π* transition [S8-S10]. Compared with the UV intensity of GO in pure water, the intensity of GO in $FeCl_3$ solution markedly decreased, indicating that the conjugate double bonds of the aromatic group in GO are greatly affected in the $FeCl_3$ solution, which is consistent with our theoretical computations.

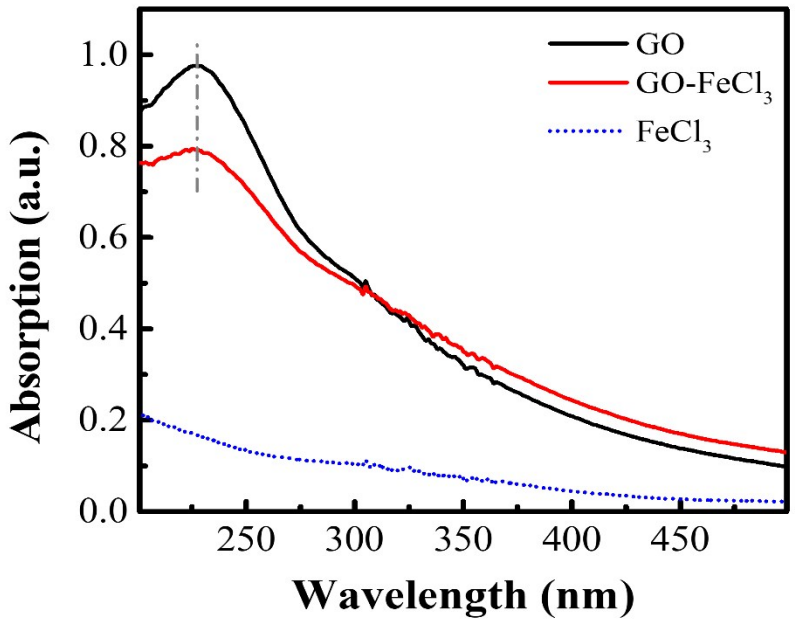

Supplementary Fig. S14. UV absorption spectra of GO suspension (50 mg/L) 1:1 mixed with $FeCl_3$ solution (5 mg/L).

PS16: Effect of anions on permeation behavior

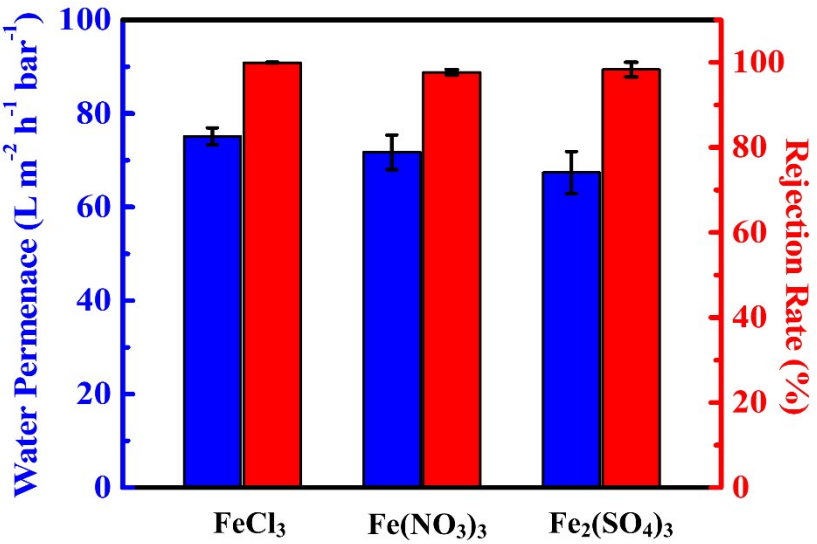

Supplementary Fig. S15. Water permeances and rejection rates for the GO membranes with different anions.

PS17: Rejection performance of mixed-ion permeations though the GO membrane without cationic control

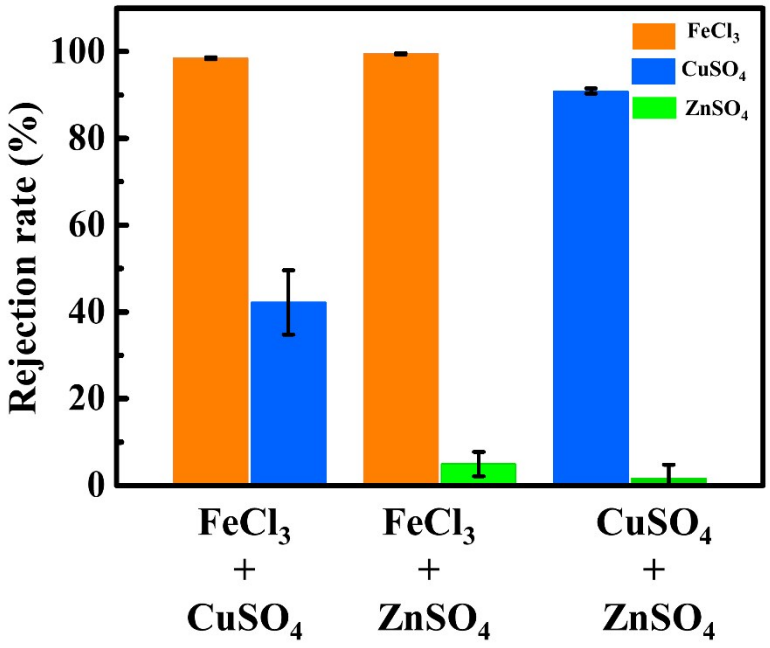

Supplementary Fig. S16. Rejection performance of mixed-ion permeations though the GO membrane without cationic control.

References

S1. Hummers, et al. Preparation of Graphitic Oxide. *J. Am. Chem. Soc.* **1958**, *80*, 1339.

S2. Xu, Y., et al. Flexible graphene films via the filtration of water-soluble noncovalent functionalized graphene sheets. *J. Am. Chem. Soc*. **2008**, *130*, 5856-5857.

S3. Pan, D., et al. Li Storage Properties of Disordered Graphene Nanosheets. *Chem. Mater*. **2009**, *21*, 3136-3142.

S4. Becke, A. D. Density-functional exchange-energy approximation with correct asymptotic behavior. *Phys. Rev. A* **1988**, *38* (6), 3098-3100.

S5. Lee, C., et al. Development of the Colle-Salvetti correlation-energy formula into a functional of the electron density. *Phys. Rev. B* **1988**, *37* (2),785-789.

S6. Gaussian 09, Revision D. 1, Frisch, M. J., Trucks, G. W., Schlegel, H. B., Scuseria, G. E.,Robb, M. A., Cheeseman, J. R., Scalmani, G., Barone, V., Mennucci, B., Petersson, G. A., Nakatsuji, H., Caricato, M., Li, X., Hratchian, H. P., Izmaylov, A. F., Bloino, J., Zheng, G., Sonnenberg, J. L., Hada, M., Ehara, M., Toyota, K., Fukuda, R., Hasegawa, J., Ishida, M., Nakajima, T., Honda, Y., Kitao, O., Nakai, H., Vreven, T., Montgomery, J. A., Jr., Peralta, J. E., Ogliaro, F., Bearpark, M., Heyd, J. J., Brothers, E., Kudin, K. N., Staroverov, V. N., Kobayashi, R., Normand, J., Raghavachari, K., Rendell, A., Burant, J. C., Iyengar, S. S., Tomasi, J., Cossi, M., Rega, N., Millam, J. M., Klene, M., Knox, J. E., Cross, J. B., Bakken, V., Adamo, C., Jaramillo, J., Gomperts, R., Stratmann, R. E., Yazyev, O., Austin, A. J., Cammi, R., Pomelli, C., Ochterski, J. W., Martin, R. L., Morokuma, K., Zakrzewski, V. G., Voth, G. A., Salvador, P., Dannenberg, J. J., Dapprich, S., Daniels, A. D., Farkas, Ö., Foresman, J. B., Ortiz, J. V., Cioslowski, J., Fox, D. J. Gaussian, Inc., Wallingford CT, **2009**.

S7 Zhang M. et al. Controllable ion transport by surface-charged graphene oxide membrane. *Nat. Commun*. **2019**, *10*, 1253.

S8. Shi, G. et al. Unexpectedly Enhanced Solubility of Aromatic Amino Acids and Peptides in an Aqueous Solution of Divalent Transition-Metal Cations. *Phys. Rev. Lett.* **2016**, *117*, 238102.

S9. Chuang, C. H. & Chen, Y. T. Raman scattering of L-tryptophan enhanced by surface plasmon of silver nanoparticles: vibrational assignment and structural determination. *J. Raman Spectrosc.* **2009**, *40*, 150-156.

S10. Yorita, H. et al. Evidence for the cation-π interaction between Cu^{2+} and tryptophan. *J. Am. Chem. Soc.* **2008**, *130*, 15266-15267.